DOI: https://doi.org/10.68732/3e60f4b6aae8bed8

ISBN: 978-9989-2053-6-1

Permeability and acoustic emission response characteristics during injection-induced fault slip

Ke Zhang[1,2], Qiang Li[1,2], Yueqiang Ma[1,2], Sida Jia[1,2], Jinsen Li[1,2] Quan Gan[1,2], Derek Elsworth[3]

[1]*State Key Laboratory of Coal Mine Disaster Dynamics and Control, Chongqing University, Chongqing, China*
[2]*School of Resources and Safety Engineering, Chongqing University, Chongqing, China*
[3]*Department of Energy and Mineral Engineering, EMS Energy Institute and G3 Center, Pennsylvania State University, University Park, PA, USA*

quan.gan@cqu.edu.cn
0000-0001-5201-8817

Abstract

Here we performed fluid injection experiments on granite samples containing smooth faults under varying initial critical stress states. Results demonstrate that the initial critical stress state exerts first-order control on seismic activity, with critically stressed faults exhibiting stronger seismic responses during activation. During injection, the pressure rapidly increases and then stabilizes at a constant level. Under different critical stress conditions, injection-induced reactivation of faults will result in a different acoustic emission response. Slip events occur abruptly, highlighting the sudden and destructive nature of injection-induced unstable slip. We found that faults closer to critical instability exhibited shorter failure durations, manifested as AE signals concentrated within a narrower time window. This work elucidates how initial fault stress governs the co-evolution of permeability and acoustic emission response, advancing understanding of injection-induced seismicity physics.

Keywords

Injection-induced seismicity, Stress state, Permeability, Acoustic emission.

1 Introduction

Injection-induced seismicity has become a globally pervasive geophysical phenomenon that poses significant challenges for subsurface engineering applications, especially enhanced geothermal systems (EGS), shale gas wastewater reinjection, and CO_2 sequestration projects (Ellsworth 2013). The current mechanistic understanding of injection-induced seismicity includes multiple coupled processes, pore pressure diffusion, thermal-water-mechanical interactions, seismic wave triggering, and aseismic slip transients (Guglielmi et al. 2015). Of these, pore pressure diffusion through fault zones is widely recognized as the predominant triggering mechanism (Shapiro et al. 2011), with elevated fluid pressures lowering the effective normal stress and facilitating fault reactivation (Elsworth et al. 2016). The dynamic interplay between permeability evolution and induced seismicity during high-pressure fluid injection is particularly important for optimizing EGS reservoir performance, ensuring the integrity of the nuclear waste repository, and advancing physics-based seismic hazard assessment (Woo et al. 2019). Field observations and laboratory experiments have consistently demonstrated that injection-induced sliding events exhibit complex magnitude-frequency distributions modulated by coupled hydrodynamic processes (Passelègue et al. 2018).

The initial stress state of the fault is a key factor controlling the seismic activity by injection induced (McGarr 2014). The traditional theory, based on the assumption of moderate stress state, has established a fundamental theoretical framework between the release of seismic moments and the injected volume (Galis et al. 2017). Field observations and experimental studies have shown that stress states of many faults are closer to the critical instability conditions, which makes the classical model based on the assumption of moderate stress have obvious limitations in predicting actual seismic activities (Li et al. 2021). Faults under different initial stress states exhibit distinct response to fluid injection. This is not only reflected in the scale of seismic moment release but also affects the suddenness of instability and the mode of rupture propagation.

The evolution of fault permeability also plays a critical role in injection-induced seismicity. As a key parameter governing pore pressure diffusion and fluid migration pathways, dynamic changes in permeability directly influence the redistribution of effective stress and the destabilization process of faults. Seismic events exert multifaceted control over hydrogeological systems by affecting dynamic permeability; seismic waves generated by seismic activity led to either increased or decreased permeability. The magnitude-frequency distribution provides a fundamental framework for the statistical patterns of seismic activity, typically described by the Gutenberg-Richter law (Gutenberg and Richter 1944). According to this law, a negative correlation exists between earthquake magnitude and occurrence frequency, corresponding to a low frequency for large magnitudes and a high frequency for small magnitudes (Tormann et al. 2015).

We conducted fluid injection tests on granite samples containing smooth artificial faults, with pre-loaded strengths at 80%, 84%, 88%, and 92% of peak shear strength. Faults closer to the critical instability state exhibited greater stress drop and higher peak slip rates.

2 Materials and Methods

Fluid injection experiments were conducted on fractured granite samples. The granite primarily consists of quartz (33%), feldspar (62%), and mica (5%), with an average grain size of approximately 2 mm. The granite exhibits a porosity of about 0.6% and macroscopically uniform texture. Experimental results measured using the pressure pulse decay method indicate an intrinsic permeability of 1.3 μD for the granite matrix. Granite samples with a diameter of 50 mm and height of 100 mm were cut at a 30° angle to the core axis, ensuring each sample contained a smooth fault inclined at 30° to the axial direction. Two drill holes with a nominal diameter of 2.5 mm were drilled in parallel along the vertical direction near the fault surface at the end of the sample, to allow fluid flow from the core holder inlet into the fracture and subsequently to the exit hole, which was 5 mm from the edge of the sample. The samples were fixed within the core holder using two layers of polytetrafluoroethylene and separated from the surrounding oil.

The fluid-driven fault reactivation experiment was carried out by using a high-temperature and high-pressure triaxial fault shear permeability test system at ambient temperature (20°C), and using silicone oil and distilled water as the enclosing fluid and injection fluid, respectively. The normal stress (σ_n) and shear stress (τ) of the fracture are calculated as:

$$\sigma_n = \sigma_3 + (\sigma_1 - \sigma_3)cos^2\psi \quad (1)$$

$$\tau = (\sigma_1 - \sigma_3)\sin\psi\cos\psi \quad (2)$$

where σ_1 is the axial stress, σ_3 is the confining stress, and the sampling frequency is 10 Hz; σ_1-σ_3 are the deviatoric stresses measured directly by the pressure measuring element in the vessel; ψ is the inclination angle of the fracture relative to the core axis. Since the pore pressure interacts with the positive stress on the fracture surface, the effective normal stress is calculated as:

$$\sigma_{eff} = \sigma_n - P_{pore} \quad (3)$$

During fluid injection, the normal and shear stresses on the fracture are maintained by controlling the axial and peripheral pressures through a servo system. The shear displacement along the fracture (d_{slip}) is calculated as:

$$d_{slip} = \frac{d_l}{\cos\psi} \quad (4)$$

where d_l is the load point displacement, measured in a triaxial fault shear permeability test equipment vessel. The evolution of permeability (k) at rock fractures was calculated based on the cubic law:

$$k = \frac{e_h^2}{12} \quad (5)$$

where e_h is the fracture aperture (m) at the fracture surface. In this study, it is considered that the fluid flows only at the fracture surface thus leading to induced shear slip, and the fracture aperture is calculated as:

$$e_h = \left[-\frac{12\eta LQ}{w(P_{in} - P_{out})}\right]^{\frac{1}{3}} \quad (6)$$

where Q is the steady-state flow rate (m^3/s), P_{in}-P_{out} (ΔP) is the pressure difference, and η is the fluid viscosity (1.002×10^{-3} Pa-sec for distilled water at 20°C).

3 Results

3.1 Injection-induced slip behaviour is controlled by vary initial critical stress state of the fault

The initial stress state of faults governs the pattern and intensity of injection-induced fault reactivation. Under constant confining pressure σ_3=11 MPa and injection pressure p=1 MPa, granite specimens containing smooth interfaces inclined at 30° relative to the core axis were subjected to axial loading. This led to a progressive increase in resolved shear stress with slip until it reached 92%/88%/84%/80% of the peak shear strength τss. In the second stage, we maintained a fixed axial piston position to ensure zero displacement conditions at both ends of the granite specimens. Fluid injection then commenced at a rate of 1 MPa/min, increasing from 1 MPa to 10 MPa. Due to the high permeability of the fracture surfaces, fluid pressure rapidly reached millisecond-scale equilibrium within the specimens. During fluid injection, both representative sample sets exhibited distinct dynamic slip events throughout the pressure ramp, characterized by rapid shear stress decline and abrupt displacement increase.

The dependence of injection-induced seismicity on the initial stress state of faults is summarized visually in Fig.1. The stress drop decreases from 1.38 MPa at 92% critical stress to 0.84 MPa at 80% critical stress. The injection pressure required to induce instability is inversely proportional to the fault's initial stress state. Faults with a critical stress of 92% slip when injection pressure to 4.1~4.7 MPa, whereas faults with an initial stress state of 80% require a greater injection value to slip.

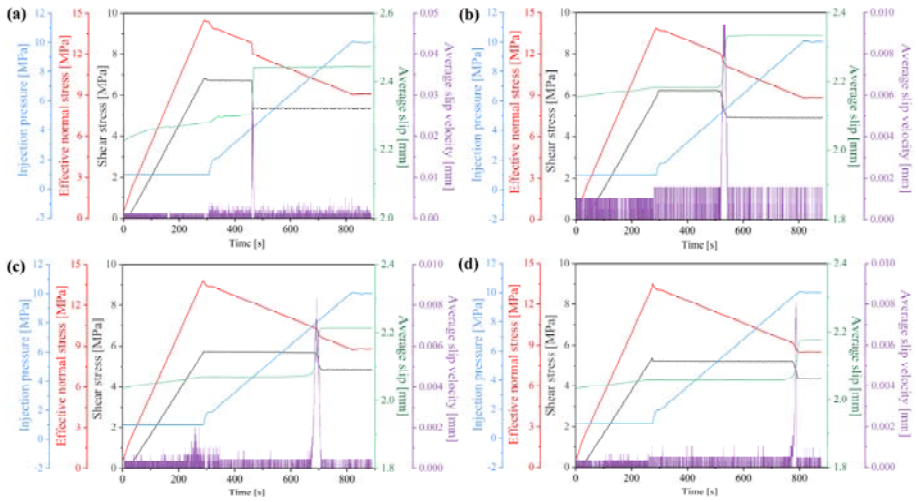


Fig. 1 Mechanical behavior of injection - induced fault slip under vary critical stress states. (a), (b), (c), (d) shows the mechanical behavior across 92% / 88% / 84% / 80% critical stress states.

To sum up, our results jointly depict the continuous spectrum of the fault slip mode controlled by the initial stress state. There is a common trend that faults closer to the critical instability state exhibit more intense seismic slip instability, characterized by greater stress drop, faster sliding speed, earlier instability occurrence time and lower trigger pressure. In contrast, faults preloaded to lower stress levels exhibit progressive quasi-static sliding responses.

3.2 Characteristics of injection-induced failure mode

Fig.2 illustrates the AE response characteristics of injection-induced fault slip. Results indicate that the AE response intensifies as the initial stress state of smooth faults approaches critical instability (e.g., 92% τ_{ss}). For smooth faults, the maximum AE energy increased significantly from 109.25 mV*ms to 139.83 mV*ms as the initial stress rose from 80% to 92%, while the ring-down counts (RDC) also increased from 28 to 39. This systematic increase in AE energy reveals that fault reactivation under higher stress states generates higher-energy microfracture activity, indicating a more violent brittle failure process. Furthermore, the initial stress state significantly influences the temporal characteristics of instability events. We found that faults closer to critical instability exhibited shorter failure durations, manifested as AE signals concentrated within a narrower time window. This indicates that fault instability under high stress states exhibits greater suddenness and faster fracture propagation speeds.

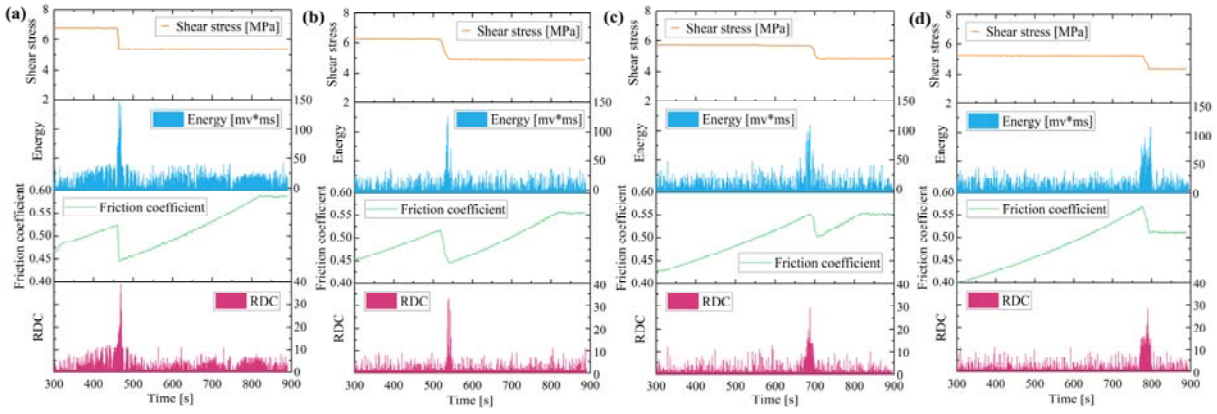


Fig. 2 AE characteristics of injection-induced fault slip process. (a), (b), (c), (d) shows the mechanical behavior across 92% / 88% / 84% / 80% critical stress states

The most direct mechanism for injection-induced fault slip is the reduction in closure pressure due to increased pore pressure. Once reactivated, the fault's frictional response may lead to stable slip or unstable slip. In this study, smooth faults exhibited dynamic slip during injection-induced failure, with the friction coefficient abruptly decreasing from the static to kinetic value.

4 Discussion

When fault instability occurs, permeability exhibits rapid growth (Fig.3). Sustained diffusion under high pore pressure reactivates faults previously at critical stress states. Dynamic slip events cause rock fracture expansion, facilitating fluid flow through fracture pathways and thereby increasing permeability. We estimated the *b*-value during the experiment using the maximum likelihood method and calculated its standard error σ(*b*). The data shows the temporal trend of *b*-value during the experiment, with black error bars representing the standard error. The abrupt decrease in b-value corresponds to a sudden increase in permeability, dropping from 1.42±0.1 during background events to 0.78±0.1 during slip events. Notably, the continuous decline in the b-value exhibited precursor characteristics earlier than the abrupt change in permeability. This advance time systematically increased with decreasing initial critical stress state, extending from 4 seconds at 92% critical stress to 15 seconds at 80% critical stress. Furthermore, faults closer to failure exhibited greater increases in permeability during slip events. Following slip events, the experimental system entered a new stable state where permeability stabilized. Cracks reached a new equilibrium post-slip, and the stabilization of flow pathways eliminated severe permeability fluctuations.

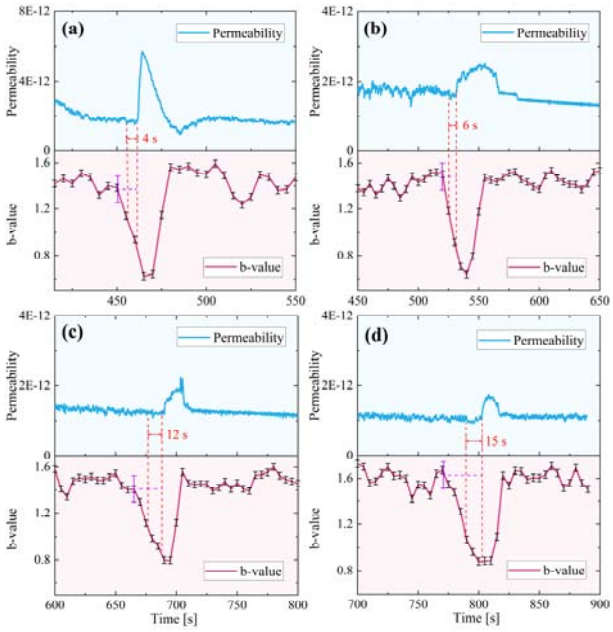


Fig. 3 Permeability and *b*-value characteristics of injection-induced fault slip process. (a), (b), (c), (d) shows the mechanical behavior across 92% / 88% / 84% / 80% critical stress states.

Through meticulous experimental design, we systematically monitored the dynamic changes of permeability and b value during the microseismic activity stage. The experimental results reveal the connection between fluid injection and fault slip behavior under vary stress states. With the continuous injection of fluid, the fluid seeps through the fissures and eventually enters the slip zone, inducing the slip of the fault.

5 Conclusions

We conducted triaxial shear permeability tests on smooth-jointed granite samples to understand the mechanism of injection-induced seismicity under different initial stress states of faults. We reveal that the initial critical stress state of faults exerts primary control over seismic activity. During injection operations, the injection pressure rapidly increases before stabilizing at a constant level for fluid injection. Slip events occur abruptly, reflecting the sudden and destructive nature of injection-induced unstable slip. We found that faults closer to critical instability exhibited shorter failure durations, manifested as AE signals concentrated within a narrower time window. Concurrently, shear stress variations demonstrate fluid injection's impact on fault stability, with pore pressure increases initially causing a slight decrease in shear stress and a rapid drop during slip events.

References

Ellsworth, W.L. (2013). Injection-induced earthquakes. Science 341 (6142), 1225942.

Guglielmi, Y., Cappa, F., Avouac, J.-P., Henry, P., Elsworth, D. (2015). Seismicity triggered by fluid injection–induced aseismic slip. Science 348 (6240), 1224–1226.

Shapiro, S.A., Krüger, O.S., Dinske, C., Langenbruch, C. (2011). Magnitudes of induced earthquakes and geometric scales of fluid-stimulated rock volumes. Geophysics 76 (6), WC55–WC63.

Elsworth, D., Spiers, C.J., Niemeijer, A.R. (2016). Understanding induced seismicity. Science 354 (6318), 1380–1381.

Woo, J.U., Kim, M., Sheen, D.H., Kang, T.S., Rhie, J., Grigoli, F., Ellsworth, W.L., Giardini, D. (2019). An in-depth seismological analysis revealing a causal link between the 2017 Mw 5.5 Pohang earthquake and EGS project. J. Geophys. Res. 124, 13060–13078.

Passelègue, F. X., Brantut, N. & Mitchell, T. M. (2018). Fault reactivation by fluid injection: controls from stress state and injection rate. Geophys. Res. Lett. 45, 837–846.

McGarr, A. (2014). Maximum magnitude earthquakes induced by fluid injection. J. Geophys. Res.: Solid Earth 119, 1008–1019.

Galis, M., Ampuero, J.P., Mai, P.M., Cappa, F. (2017). Induced seismicity provides insight into why earthquake ruptures stop. Sci. Adv. 3 (12), eaap7528.

Li, Z., Elsworth, D., Wang, C. et al. 2021. Constraining maximum event magnitude during injection-triggered seismicity. Nat Commun 12, 1528. https://doi.org/10.1038/s41467-020-20700-4.

Gutenberg B, Richter C F. (1944). Frequency of earthquakes in California. Bulletin of the Seismological Society of America, 34(4): 185-188.

Tormann, T. et al. (2015). Randomness of megathrust earthquakes implied by rapid stress recovery after the Japan earthquake. Nat. Geosci. 8, 152–158.